Earthquake Activity of Peru[1]

LEONIDAS OCOLA[2]

Geophysical and Polar Research Center
Department of Geology, University of Wisconsin, Madison

Abstract. A direct logical extension of Saint-Amand's area-average concept of strain release is the concept of volume average of strain release, here called 'specific strain release.' This extension is used to analyze the spatial distribution of the seismic activity of Peru between January 1947 and July 1963. When specific strain is projected and summed on a vertical axis, three distinct seismic zones are found in the Peruvian upper mantle. The first, from near surface to 300 km, contains the majority of events and most of the strain release. The second zone, 300–500 km, contained no seismic activity during the 14½ years considered. The third zone, 550–750 km, is characterized by high activity centered at about 640–650 km. The activity within the first zone, when projected to the surface, appears to be concentrated in two major belts, each consisting of two linear segments. The western belt (the more active) lies between the Andean block and the Peru-Chile trench. The eastern belt lies east of the Andean Mountains and west of the border of the Brazilian shield. The common linear segments of these belts are broken and turn about 30° in a zone of low seismic activity marked by a similar change in the angle of the Andes, the offshore trench, and the surface fault system, and by the discordant junction of the oceanic Nazca Ridge with the continent. The distribution of the seismic activity in cross projection suggests the existence of several 'high-activity bands' contributing to each belt. These bands agree in dip and strike with fault-plane solutions for earthquakes within them. The depth distribution of the specific strain release, and the theoretical rate of accumulation of thermoelastic stress for an earth with acceptable horizontal and vertical temperature gradients, are generally proportional in depth within the upper 300 km. Although many earthquake mechanisms might exist, Benioff's collapse and Orowan's creep instability mechanism seem to be consistent with narrow horizontal bands of high activity found for the deepest shocks.

INTRODUCTION

This paper deals with the development of a quantitative method for studying the spatial distribution of seismic activity, and its application to Peru. The method provides techniques leading to the identification and delineation of active structures or high-activity bands in terms of the seismicity size parameter. Through projection to the earth's surface and to other planes appropriate in orientation, the method allows comparison of the distribution of seismic activity with models of the earth's mantle from other fields of study [*Ocola*, 1966].

Among the most important advances that make this investigation possible are: (1) the introduction of the concept of surface area average for the study of earthquake strain release, made by *Saint-Amand* [1956], (2) the almost general acceptance of the magnitude as a measure of the size of earthquakes, and (3) the systematic determination of earthquake magnitude by means of the Richter-Gutenberg scale made by the worldwide centers.

The most important improvements in quality spring from advances in instrumentation, especially in sensitivity and time keeping, and from the increased numbers of teleseismic stations reported to worldwide seismic centers. High-speed computers, which can provide the large number of solutions necessary, have at least doubled the number of computed earthquake locations from the number previously available, and, with the continuing international cooperation in earthquake reporting, have enormously improved the accuracy of hypocenter location.

[1] Contribution 169, Geophysical and Polar Research Center, Department of Geology, University of Wisconsin.

[2] On leave from Instituto Geofísico del Peru.

SEISMICITY PARAMETERS

Webster defines seismicity as the 'state, quality, or degree of being seismic; relative liability to earthquakes; specifically, the frequency of earthquakes occurring in a given region as measured by the ratio between the total number of recorded earthquakes and the area in square miles.' We consider 'the state, quality, or degree of being seismic' as the most appropriate definition of seismicity. However, the portrayal of seismicity should take into account not only the number of recorded events but also their size, frequency, and spatial distributions, as well as their mode of occurrence. Keeping some of these considerations in mind, we will deduce systematically explicit expressions that will improve the portrayal of the 'degree of being seismic.'

Let F stand for some function of the mean number of earthquakes (η) in a bounded region and G for some function of their mean relative or absolute size (ξ); then the seismicity of any region can be characterized by

$$S = S[F(\eta), G(\xi), t] \tag{1}$$

where t is time.

The simplest functional relationship between $F(\eta)$ and η, and $G(\xi)$ and ξ, is given by

$$F(\eta) = \eta \quad \text{and} \quad G(\xi) = \xi \tag{2}$$

Since η and ξ are not known, they are estimated from the observed data in the form of averages.

An estimate of the parameter η is given by

$$\eta_P(N) = \frac{K}{TP} \sum_T \sum_P N_{TP} \tag{3}$$

where P can be length, area, or volume for one-, two-, or three-dimensional averages; K is a proportionality constant; N is the number of earthquakes for a given T and P; and T is the number of years analyzed.

The size parameter ξ is a function of energy or strain release per unit volume per unit time. This parameter can be estimated as a function of the strain energy (E) as follows:

$$\xi_P(E) = \frac{H}{TP} \int_T \int_P E \, dp \, dt \tag{4}$$

where H is a proportionality constant.

When P = area, equation 4 was called 'specific seismicity' by *Saint-Amand* [1956]. But here it will be called area energy release, and 'specific' will be reserved for volume averages. When P = volume, equation 4 is the average energy release per unit of volume per unit time, called 'specific energy release.'

Similarly, the expressions for ξ as a function of the strain release (e) will be given by

$$\xi_P(e) = \frac{H'}{TP} \int_T \int_P e \, dp \, dt \tag{5}$$

where H' is a proportionality constant.

Benioff [1949] and *Saint-Amand* [1956] have shown that the average strain release is proportional to the square root of the energy associated with it. Hence equation 5 can be rewritten as

$$\xi_P[E^{1/2}] = \frac{C'}{TP} \int_T \int_P E^{1/2} \, dp \, dt \tag{6}$$

where C' is a proportionality constant.

When P = area, equation 6 becomes what Benioff called 'tectonic flux.' It will here be called area strain release. When P = volume, it will be called 'specific strain release,' and will represent average strain release per unit volume per unit time.

Equations 4 and 6 depend directly on evaluation of energy released by an earthquake. Although it is impossible to get absolute values for this quantity, relative values can be reached if energy is expressed in units of the energy of a reference magnitude shock which can be revised as absolute estimates improve. The previous equations can be transformed into the new scale as follows:

Let E_f be the estimated energy release for a reference magnitude or fiducial size earthquake; N_f the times E_f is contained in the energy release (E) of any earthquake. That is,

$$E = N_f E_f \tag{7}$$

Define an energy release parameter ϕ and ϵ strain release parameter as

$$\phi_P(N_f) = \xi_P(E)/E_f \tag{8}$$

and

$$\epsilon_P(N_f^{1/2}) = \xi_P(E^{1/2})/E_f^{1/2} \tag{9}$$

Then from equations 4 and 7 these parameters

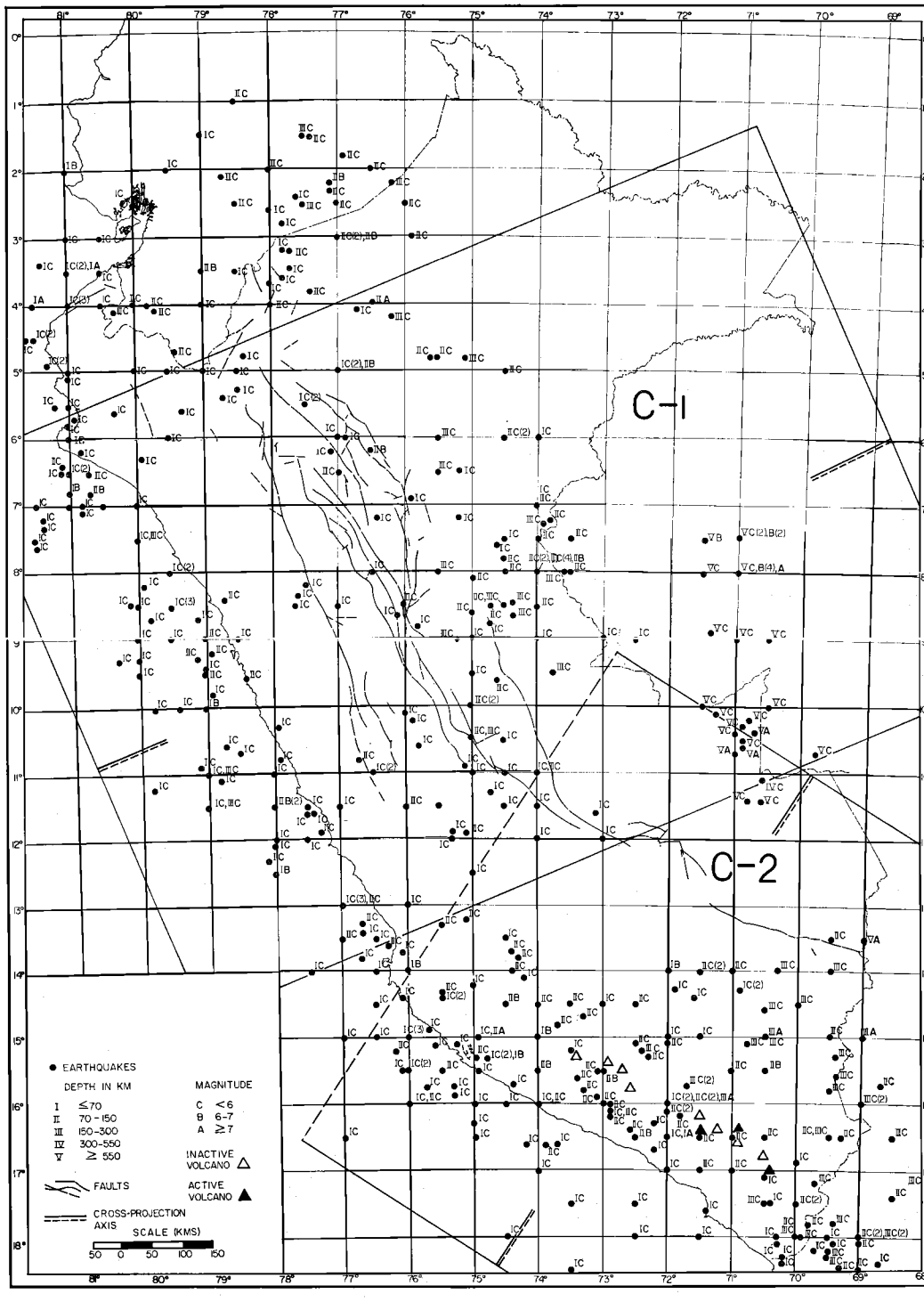

Fig. 1. Epicenter map for Peru: January 1949 to July 1963. Numbers in parentheses after magnitude groups represent the number of epicenters with the same magnitude and location. C-1 and C-2 stand for the seismotectonic blocks C-1 and C-2.

are estimated by

$$\phi_P(N_f) = \frac{H}{TP} \int_T \int_P N_f \, dp \, dt \qquad (10)$$

and

$$\epsilon_P(N_f^{1/2}) = \frac{C'}{TP} \int_T \int_P N_f^{1/2} \, dp \, dt \qquad (11)$$

The relative size parameters ϕ and ϵ are independent of absolute knowledge of the amount of energy release by earthquakes.

In what follows, we will apply the seismicity size parameter definitions to the study of a section of one of the world's most intricate areas of earthquake activity: Peru.

MATERIAL USED

Four hundred ninety earthquakes occurring during 14½ years were processed for this study of the seismic activity of Peru, 60% of them from the period January 1959 to July 1963; they are shown in Figure 1. (The author will be glad to provide the complete list of earthquakes to those needing it.) The main sources of information were the *United States Earthquake Bulletin* (U.S.C.G.S.), the *Bulletin du Bureau Central International de Séismologie* (Strasburg), *Preliminary Epicenter Determination Cards* (U.S.C.G.S.), the *Bulletin of the Seismological Society of America* (Earthquake Notes Section), and *Seismicity of the Earth* [*Gutenberg and Richter,* 1954].

Thirty-two shocks have magnitudes larger than 6.5. Those of undetermined magnitude were assumed to be of magnitude 4. Epicenters classified as normal or slightly deep by U.S.C.G.S. were assumed to be between 30 and 40 km deep. The average standard error for geographic position and depth is estimated to be smaller than 0.50° and less than 50 km. However, when using an averaging technique, these errors decrease by a factor of $\sqrt{N}$, provided that no systematic errors are involved, where N is the number of epicenters averaged. The accuracy of location of the high-activity centers is estimated to be better than ±30 km on the activity maps; they are more precisely located on the cross projection.

To make comparison with studies in other areas possible, strain release was computed through the following equation from *Gutenberg and Richter* [1956*a*]

$$\log E = 11.8 + 1.5M \qquad E \text{ in ergs} \qquad (12)$$

From equations 7 and 12 for a reference magnitude of size 4 the following relation is obtained:

$$\log (N_4^{1/2}) = 0.8(M - 4) \qquad (13)$$

where N_4 is the number of equivalent earthquakes of magnitude 4. The energy was computed using the quadratic form

$$\log E = 9.4 + 2.14M - 0.054M^2 \qquad E \text{ in ergs} \qquad (14)$$

[*Gutenberg and Richter,* 1956*b*].

RESULTS

Successive projections onto maps showing epicenters, strain release, and energy release, and onto cross projections and one-dimensional profiles, seem to be the clearest way to summarize the results of this study.

1. *Epicenter map.* An epicenter map plots epicenters and information about magnitude and depth of earthquakes. When epicenters are numerous, they are usually coded in groups according to their magnitude and/or depth. Figure 1 shows earthquakes distributed in five groups according to their depth, and in three classes according to their magnitude (the significance of 'C-1' and 'C-2' will be discussed shortly). The most important features of this map are:

i. Epicenters of group I (less than 70 km deep) occur in the entire active area, except in the region of group V (deeper than 550 km).

ii. There is a high concentration of epicenters of groups I, II, and III (less than 300 km) in a narrow band 100 to 150 km wide along the coast. This band is under the continental shelf in area C-1 and under the continent in area C-2.

iii. In area C-1, the activity on the continent is concentrated east of the intermontane fault system, leaving an area with few epicenters between the fault system and the coast.

iv. There is a clear gap in the distribution of epicenters along parallel 13°S. This gap will be called the geographic discontinuity.

v. Epicenters of group V, occurring in a narraw band less than 150 km wide bearing N10–

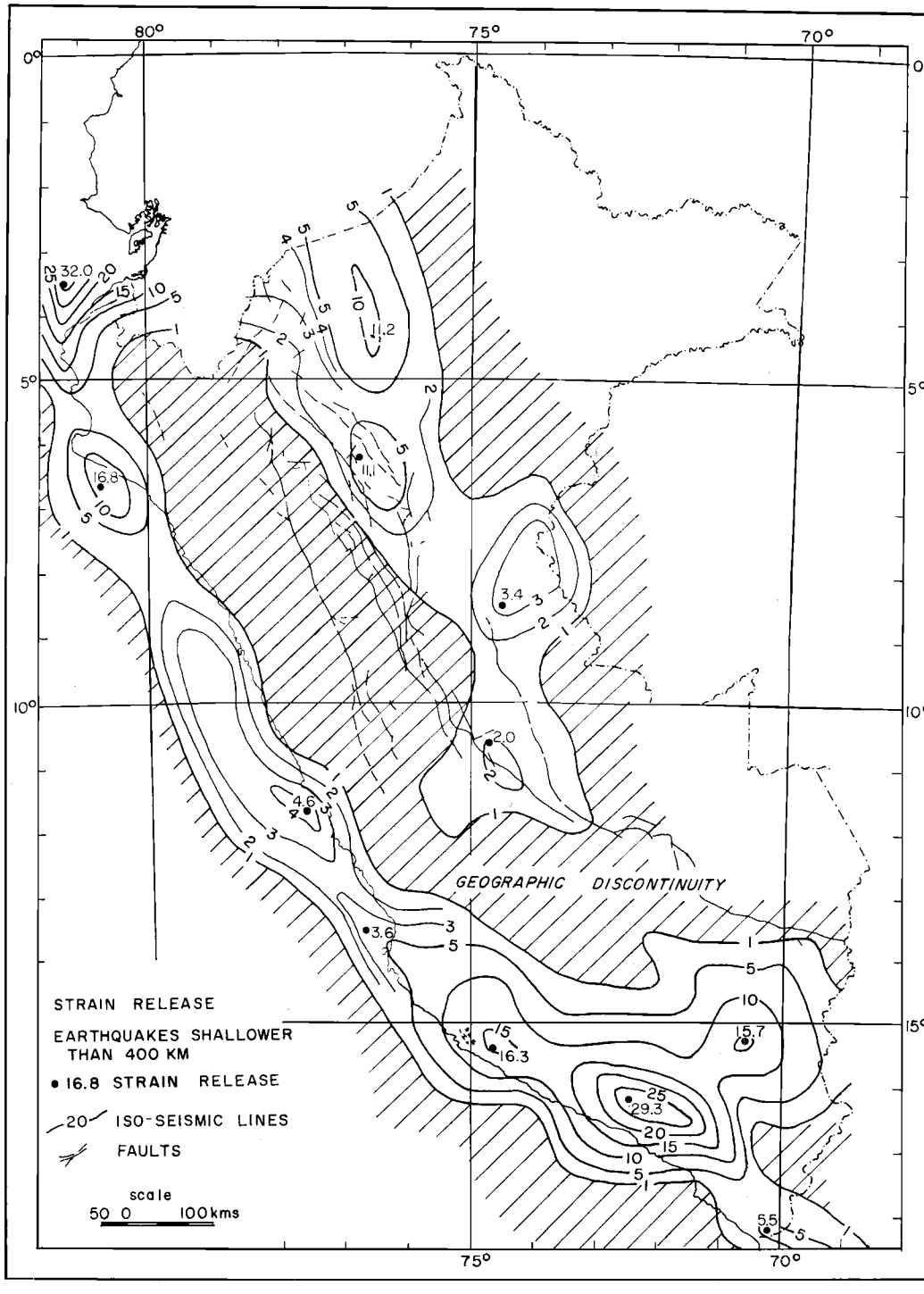

Fig. 2. Strain release map of Peru: January 1949 to July 1963. Contours and seismic groups in units of $\Sigma N_4^{1/2}$ per 1° latitude by 1° longitude per year.

15°W in area C-1 and about N40°W in area C-2. This group represents the easternmost seismic activity of Peru. During the period of analysis most of the epicenters in this group constituted a rather compact set between parallels 7°S and 11½°S.

Epicenter presentation can be used advantageously in areas of fairly small concentration where the pattern of focal depth varies so as to be clearly portrayable. But when the area of interest is one of high activity and depths are not clearly systematic, it can become confusing and uninformative.

2. *Strain release map.* This difficulty can be partly overcome if a strain release map, showing the areal distribution of parameters dependent on earthquake size and frequency, is constructed either for the complete period of observation or for means per unit time. It is more meaningful than a map showing only the number of events, and it is used in this study, with the epicenter and the energy release maps, to decide the limits and strike of the seismotectonic blocks (see below). It is a powerful tool in outlining the general trends of earthquake areas. Figure 2 shows values from the square root of the energy release per unit area per year. The unit of energy equals a magnitude 4 earthquake, and the unit of area, a rectangle 1° (latitude) by 1° (longitude). The seismic activity can be divided into two major belts, a coastal or western, and a continental or eastern. The western belt, narrow, continuous, and well defined, borders the coast northwest to southeast, from southern Ecuador to northern Chile. The eastern belt is broad and broken in two segments by the geographic discontinuity, which follows an east-west path along parallel 13°S.

The western belt is characterized by high seismic activity, in the south mainly under the continent, and in the north mainly under the continental shelf. Centers of high activity are listed below according to location. (Place names refer to the nearest city.)

i. 18°S, 72°W (Arica), a narrow strip with peak value of about 6, in units of $N_4^{1/2}$ per unit area per year. It continues to Chile.

ii. 16.5°S, 72°W (Arequipa), the highest seismic activity center on the continent. Its peak value is about 30. It is well developed and covers a large area. Flanking the eastern border of this elongated high is a belt of Quaternary volcanoes. The present active volcanoes are at the southeast border of this high.

iii. 15.5°S, 74.5°W (Acari), with a peak value of about 16. It is on the continent.

iv. 12.5°S, 77°W to 8.5°S, 79.5°W (Lima-Trujillo). Here the center is an elongated high with a peak value, near Lima, of about 5.

v. 6.5°S, 80.5°W (Chiclayo), a well-developed center, with a peak value of about 17. It lies off the coast on the continental shelf.

vi. 3.5°S, 81.0°W (Tumbes), a well-developed high center off the coast. The peak value is about 32. This center continues toward the north, where the contours seem to change in orientation.

In the eastern belt, the centers are distributed as follows:

i. 15.5°S, 70.5°W (Ayaviri), with a peak value of about 16. Contour 10 encloses the western Atico and Arequipa high as well. The contour 15 encloses only this area.

ii. 11°S, 74.5°W (Oxapampa), the lowest clearly defined activity center, with a peak value of only about 2.

iii. 8°S, 74°W (Pucallpa), a broad round activity center with a peak value of about 3.

iv. 6.5°S, 76.5°W (Moyobamba), a broadly ellipsoidal center with a peak value of about 11.

v. 4°S, 76.5°W (Andoas-Barranca), an elongated center with peak value of about 11. It continues toward Ecuador.

The eastern and western high-activity belts are separated in block C-1 by a broad band of low activity lying between the coast and the fault system and merging with the geographic discontinuity.

Both the orientation of the contours and the positions of the high-activity centers indicate general trends striking N30°W in area C-1, and about N60°–65°W in area C-2. These trends intersect at parallels 13°–14°S. They agree with the general trend of the fault systems, the Andean Mountains, and the Peru-Chile Trench.

3. *Energy release map.* An earthquake energy release map for Peru, similar to the strain release map, and possessing similar advantages, is shown in Figure 3. Notice that, in comparison with Figure 2, it gives more emphasis to centers of maximum activity. The general trend of the contours and the alignment of the highs agree with those of the strain release map. The activity peaks in Figure 3 are shifted no more

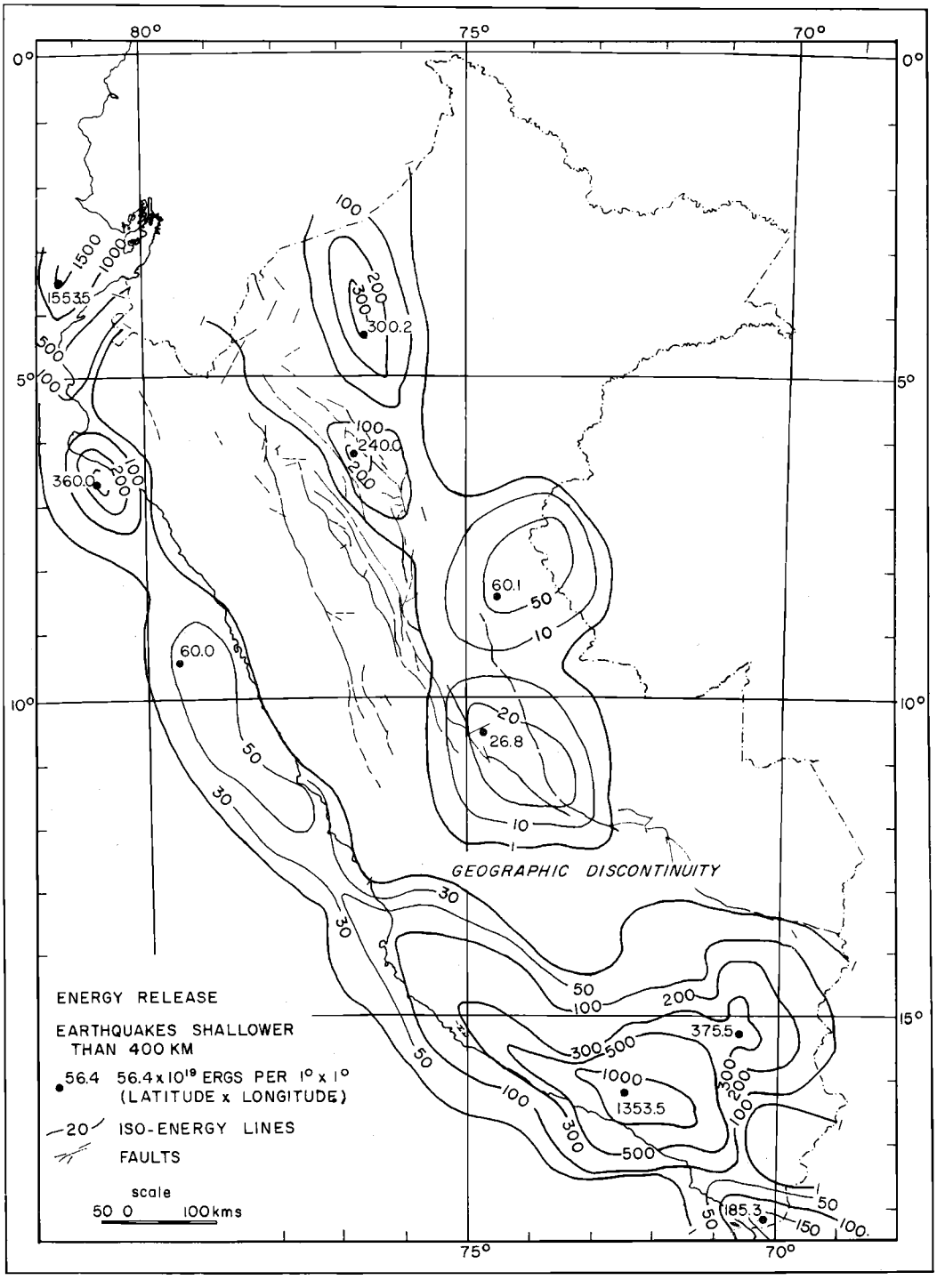

Fig. 3. Earthquake energy release, January 1949 to July 1963. Energy density groups and contours in units of 10^{+19} ergs per 1° latitude by 1° longitude per 14½ years.

than 0.5° from those in Figure 2. The activity centers in Figure 3 correlate one-to-one with those in Figure 2.

This map was prepared mainly to show that, if we know the magnitude of the event and the relation between magnitude and energy, we can outline the earthquake activity well by using either strain release or simple energy release. Notice that in the present case we have used a different scale of time and a different relation between energy and magnitude.

4. *Seismotectonic blocks.* Figure 1 includes the outline of two seismotectonic blocks, enclosing the hypocenters whose epicenters have suggested the existence of linear belts of seismic activity. These blocks are assumed to be parallel and perpendicular to the linear trends, as seen in surface projection of the seismic activity. The linear trends in Figures 2 and 3 inflect 30° between 12° and 14°S latitude. North of this inflection they orient themselves N30°W in the western belt and N25°W in the eastern. South of it the western trend shifts to about N60°–65°W, and the eastern trend is not clear. Therefore, Peru may be viewed as divided into two seismotectonic blocks, in which the activity follows approximately linear patterns. The surface expressions of the two blocks are labeled C-1 and C-2, Figure 1.

The sides of C-1 that parallel the activity are oriented N25°W, and the sides of C-2 bear N60°W. They agree with the general trends of the area's major physiographic and geologic features:

i. The submarine Peru-Chile Trench oriented about N30°W in the northern area and N55°W in the southern. The inflection is about 14½°S (estimated from maps by *Fisher and Raitt* [1962]).

ii. The Andean Mountains oriented at about N32°W and N63°W in the northern and southern areas, respectively, with an inflection at about 13°S [*Hammond,* 1955].

iii. The major fault systems (the sub-Andean and Andean) bearing N26°W and N22°W in the northern area and N68°W in the southern. The sub-Andean fault system indicates an inflection at about parallel 12½°S (Figure 2).

iv. The major outcrops of intrusive rocks along the coast oriented at N20°W and N55°W in the northern and southern areas, respectively, with an inflection at about 14°S of latitude.

v. The Quaternary volcanoes in the southern area are distributed along a line N60°W.

5. *Cross projections.* A cross projection casts a parameter of seismic activity horizontally onto a vertical plane normal to the general trend of the seismic activity, so that the general trends of the contours give an estimate of the dip of the structure. It requires proper determination of strike, as the direction along which it is made is critical. A cross projection follows the same techniques as conventional maps, and like them it can be used to portray hypocenters and hypocenter density as well as energy and strain release. Using the orientations of the seismotectonic blocks, cross projections were constructed perpendicular to the strike of the activity in each block (Figures 4 and 5). The distribution of the seismic activity in block C-1 is simpler and better defined than in C-2, and its total active horizontal extent is greater and shallower than in C-2, where the activity is more heavily concentrated along the coast.

It is remarkable that the activity can be divided vertically into three major zones: (*i*) from near surface to about 300 km, (*ii*) from 300 to about 550 km, and (*iii*) from 550 to 700 km, below which it ceases completely. *Gutenberg* [1951] and *Gutenberg and Richter* [1954] also recognized this general zoning under western South America.

i. The activity in the upper zone of C-1 (Figure 4) is not uniformly distributed, but concentrated along narrow bands dipping inland. The activity belts, evident in previous maps, appear as bands of high seismic activity with the high-activity centers dipping 60°–70° northeast in the west and about 40° northeast in the east. There is a conspicuous region of low activity separating these belts.

In C-2 (Figure 5) the western high-activity band dips 70°–90° northeast. To this band belongs the so-called 'San Agustín Fault System' [*Rodríguez et al.,* 1962]. No low-activity band separates the western from the eastern high-activity band, and they merge in the upper 100 km. Below that, between Apurimac and Manú, a well-defined activity band dips about 40° northeast.

ii. The middle zone. This is an enigmatic zone about which there is no information from earthquakes. Do earthquakes occur in this

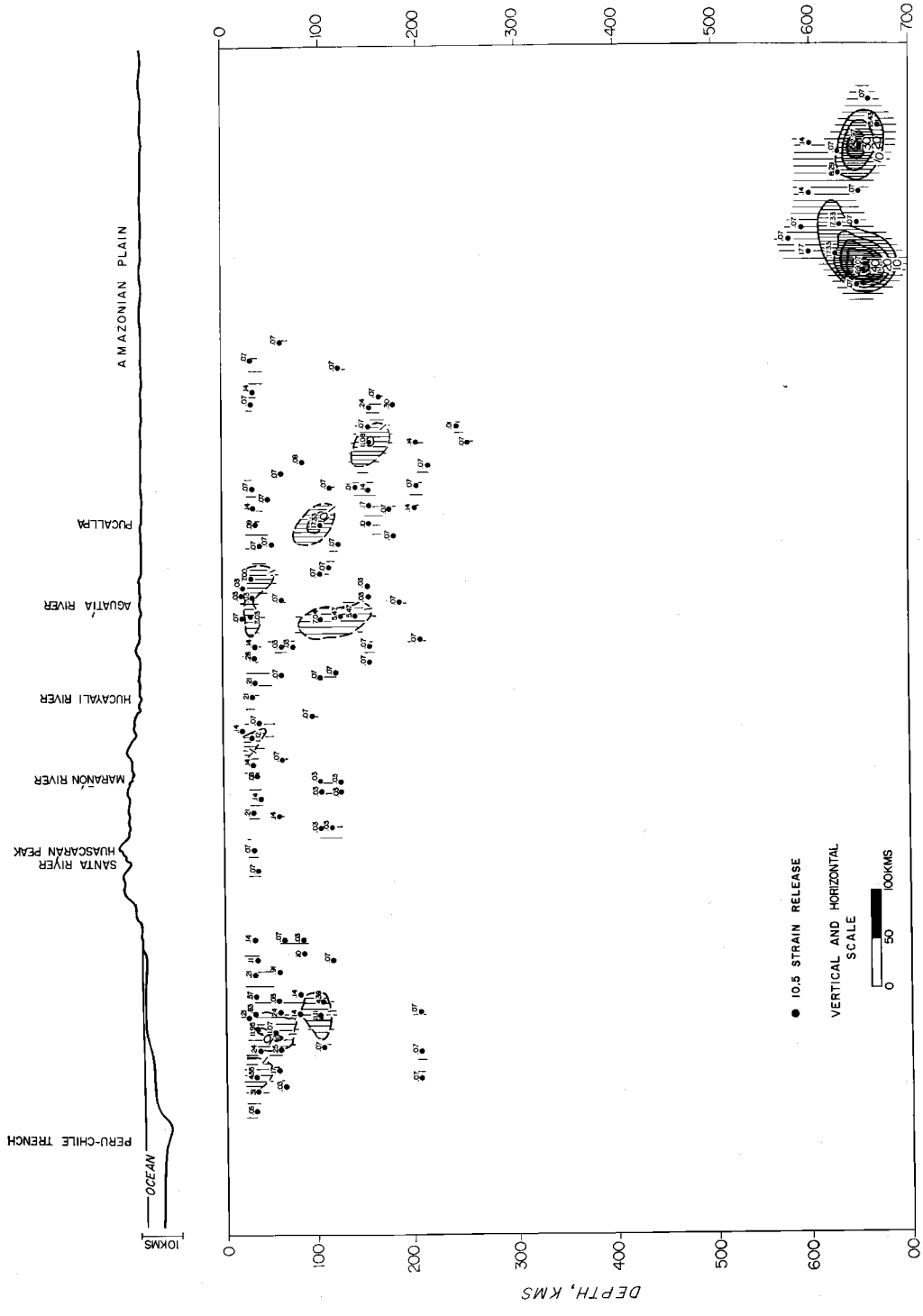

Fig. 4. Cross projection for strain release, block C-1. Contours in units of $\Sigma N_4^{1/2}$ per 20×20 km^2 per year.

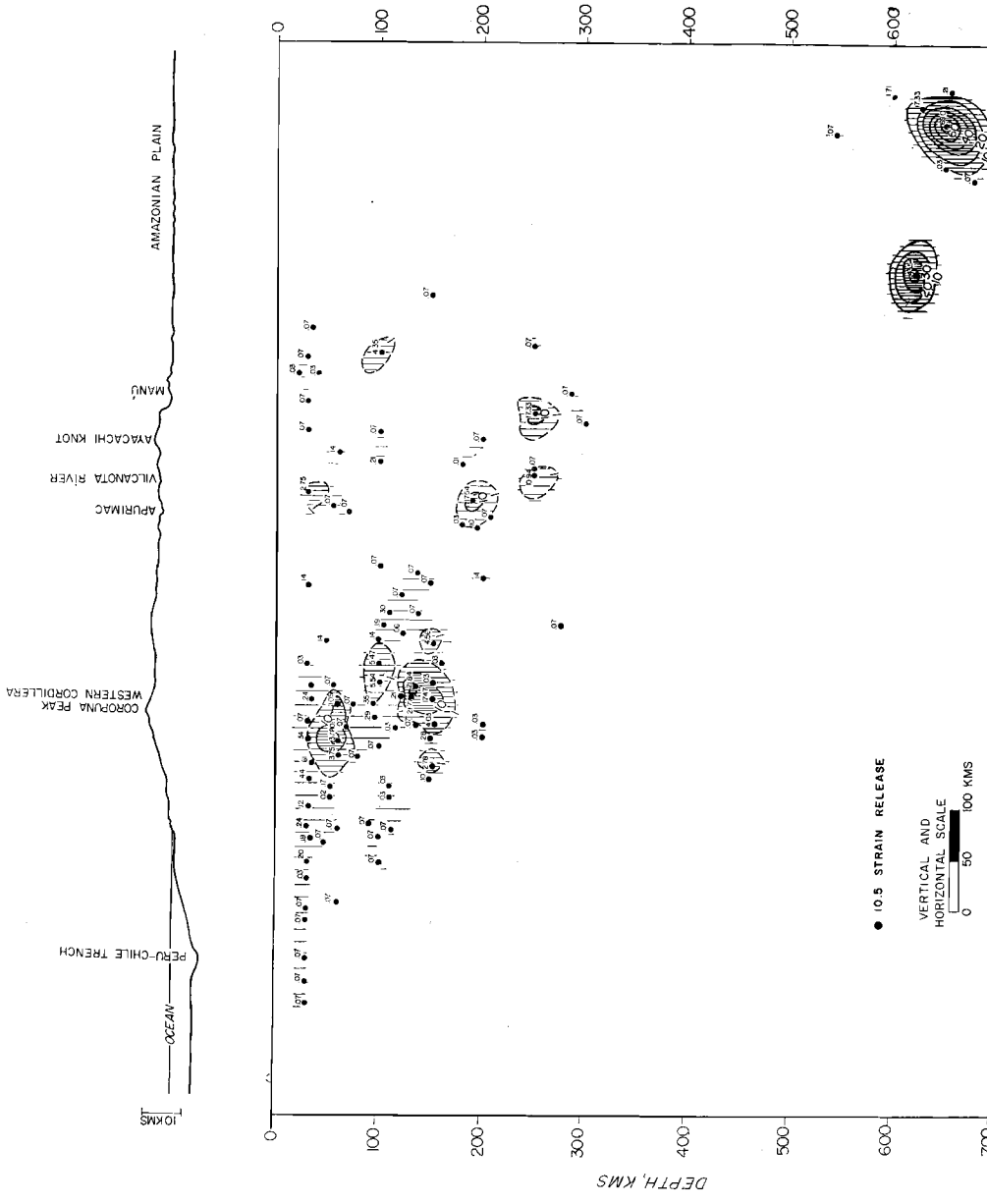

Fig. 5. Cross projection for strain release, block C-2. Contours in units of $\Sigma N_4^{1/2}$ per 20×20 km^2 per year.

zone? If they do, why are they not detected at the surface? These questions have no immediate answer.

iii. The lower zone. The epicenters of this deepest zone lie between the Andes Mountains and the Brazilian Shield. Its centers of high activity tend to be aligned horizontally in both blocks, rather than dipping steeply as is expected for the 'deep structure' of the so-called island arcs. It appears in the cross projection as a band about 150 km wide, with most of the activity being centered at 640–650 km.

6. *Projection on a vertical axis.* A projection on a vertical axis permits investigation of layering and determination of average rates of strain release (or energy release) with depth. A cumulative plot[3] of strain release is the principal technique, and it is obvious that the slope of the cumulative plot is proportional to the strain release. If such a plot can be fitted by linear segments, each segment will determine a layer where the strain (or energy) release is a constant.

The distribution of specific strain with depth for both blocks is shown in Figures 6, 7, 8, and 9. Although this distribution alone is highly suggestive for the detail known, it has to be taken with caution because of the limitations imposed by the accuracy of the earthquakes' depths and by the brevity of the period analyzed. Even so, the major features depicted in each figure are important in the over-all framework of this seismic area.

The western belt reveals some unexpected differences of depth distribution between blocks C-1 and C-2. In C-1 (Figure 6), under the continental shelf, there is a principal zone with nearly constant activity from near surface down to 120 km. In C-2 (Figure 7), on the other hand, two layers appear. The upper layer extends 110 km below the surface, with an interval of low activity at its base; then the belt's highest activity appears between 110 and 170 km. Both western blocks show a sharp cutoff marking the lower limit beyond which the seismic activity remains very slight, 210 km in C-1 and 270 km in C-2.

The eastern belt (Figures 8 and 9) shows more internal consistency than the western. The seismic activity here is distributed in three distinct layers of moderate activity. The uppermost reaches down to 80 km in C-1 (Figure 8) and to 180 km in C-2 (Figure 9), with less activity present in both blocks toward the bottom. The highest activity lies between 80 and 160 km in C-1 and between 180 and 270 km in C-2.

7. *Rate of thermoelastic stress accumulation and strain release.* Figure 10 shows the rate of strain release and the rate of thermoelastic stress accumulation. The specific strain release represents a number proportional to the total strain release per unit time. Thus it can be compared qualitatively with theoretical rates of stress accumulation with depth, to see whether there is any indication of proportionality be-

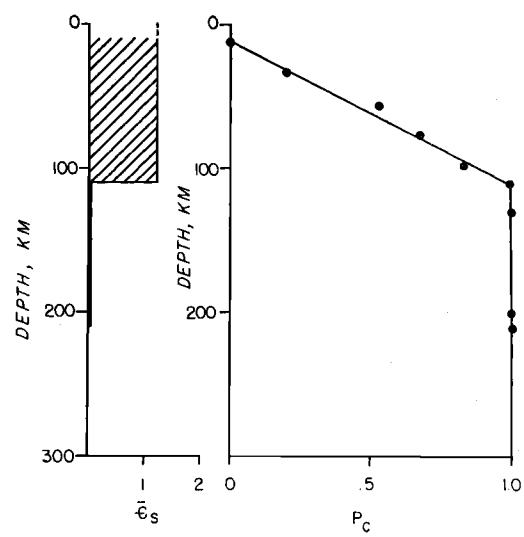

Fig. 6. Depth distribution of the specific strain release, western belt, block C-1, in units of $\Sigma N_4^{1/2}$ per unit volume per year. The unit volume is a rectangular prism with 20 × 20 km² (in the plane of cross projection) by 100 km (normal to the cross projection). *Left,* averaged specific strain release. *Right,* Cumulative plot of the specific strain release.

[3] Plot of a function of the form

$$p_n(x) = \sum_{k=1}^{n} f(\xi_k)\{g(x_k) - g(x_{k-1})\}$$

such that

$$\sum_{n=1}^{m} p_n(x) = 1 \qquad \text{for} \qquad n \leq m < \infty$$

Where $f(\xi_k)$ is a weighting function, $g(x_k)$ can be either the value of the strain or energy release, etc., at level x_k. The function $f(\xi_k)$ was assumed to be unity.

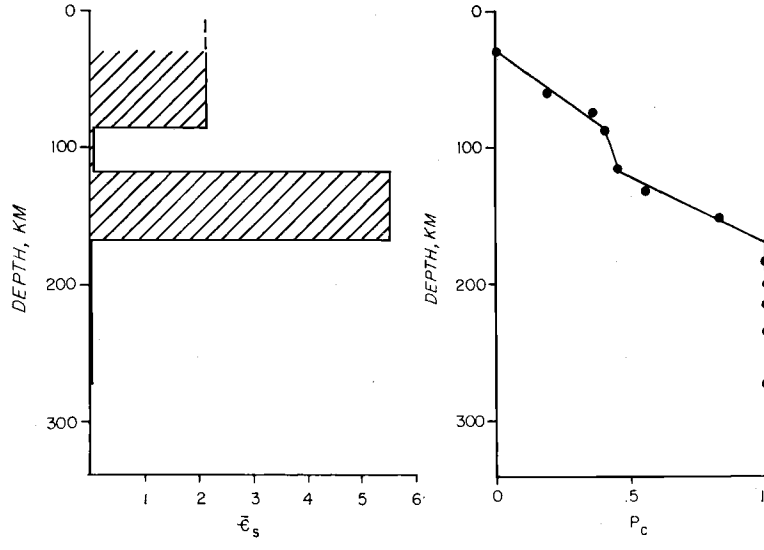

Fig. 7. Depth distribution of the specific strain release, western belt, block C-2, in units of $\Sigma N_4^{1/2}$ per unit volume per year. The unit volume is the same as in Figure 6. *Left,* average specific strain release. *Right,* cumulative plot of the specific strain release.

tween them. Since the data are sparse, it is desirable to pool the data of both blocks and to obtain average specific strain release every 50 km of depth. Figure 10 compares the results with the rate of accumulation of thermoelastic stress for an earth model with horizontal and vertical temperature gradients, computed by *Lubimova and Magnitzky* [1964]. The curves are proportional in the upper 300 km. But nothing in the theoretical curve can explain the spike in the strain release curve between 600 and 680 km.

Some statistics in zone *iii*'s (group V) earthquakes follow. The average depth of these earthquakes during the period of analysis is 634 ± 28 km. The average depth for *Benioff*'s [1949] data for South America from 1911 to 1917 is 617 ± 30 km. Pooling the two averages, the average depth of the deepest shocks is 625 ± 29 km for the 1911–1963 period. The standard deviations of these averages are smaller than the accuracy of the depths used, and they are not statistically different.

The small standard deviations of the simple averages, and the narrowness of the average specific strain release curve for these depths (Figure 10), all suggest that the deepest earthquakes in Peru occur in a narrow, nearly horizontal band. From the cross projections (Figure 5) and from Figure 1, this band appears to be 150 km wide. The maximum activity peak, based on specific strain release, not on the number of occurrences, is about 640–650 km deep.

The peak's narrowness, and its failure to correlate with the predictions from thermoelastic theory, seem to suggest that *Benioff*'s [1964] hypothesis of sudden collapse may explain their mechanism. But then the question remains, why do not earthquakes also occur all over the world at, or near, these depths, since such a mechanism depends mainly on pressure? The answer probably lies in a combination of factors.

If it is assumed that the strain energy stored in the material under the seismic regions is produced by lithostatic pressure from the weight of the overburden plus a variably deviating stress field generated by agents innate to each seismic region (potentially caused by temperature gradients, overimposed loads, different rates of convection, etc.), and assuming also that phase changes occur [*Sclar et al.,* 1964; *Ringwood,* 1962], that they occur abruptly or gradually, and that they are mainly confined to a finite depth range, then the high earthquake

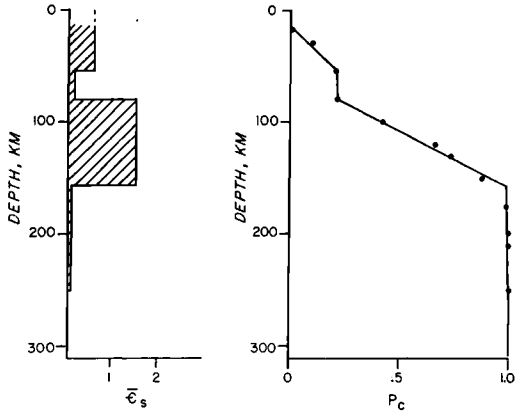

Fig. 8. Depth distribution of the specific strain release, eastern belt, block C-1, in units of $\Sigma N_4^{1/2}$ per unit volume per year. The unit volume is the same as in Figure 6. *Left,* average specific strain release. *Right,* cumulative plot of the specific strain release.

activity centered about 640–650 km depth, as illustrated by Figure 10, might be accounted for as follows:

i. Sudden phase change (*Benioff*'s [1963, 1964] collapse hypothesis) localized by a deviating stress field (possibly triggered by variation in the rate of deviating stress). Here, the sequence of events can be thought of as follows: an abrupt volume contraction produced by a phase change, migration of material from all possible directions toward the affected region, and restoration of the state of semiequilibrium. It is worth while to point out that the migration of the material will probably not be uniform in all directions, because of the existence of the deviating stress, among other factors. Owing to the collapse, a great amount of heat will be generated in the disturbed material, which will create temperature gradients contributing to the original stress field. If the amount of heat generated in this process is large enough, it might even partially reverse the original phase change. It should also be remarked that the phenomena outlined above are postulated to occur in a short period of time.

ii. Gradual phase changes and Orowan's creep fracture. It is known that a long-term stress acting on a crystalline material at either moderate or high temperatures will cause the material to creep. If a gradual phase change occurs in a particular depth range, it is to be expected that the state of creep will be altered, resulting in higher rates of creep within the range of existence of material undergoing phase change. An earthquake will occur when the material fails by creep 'fracture.' This kind of failure is postulated as a 'self-accelerating local softening of the material at an initially weak place, which may ultimately result in a shear melting' [*Orowan,* 1960].

8. *Strain release on slanted projections.* When the orientation of the seismic block is nearly correct, as evidenced by the cross projection of the active belts from which the dips of the high-activity bands are estimated, it is possible to project the seismic activity of each belt onto a plane oriented in such a way that it provides the maximum resolution. The best strike of the projection plane is given by the orientation of the normal to the cross-projection plane. In this study the high-activity belts in each block were projected individually. They are shown on Figures 11, 12, 13, and 14.

The projection of the eastern belt in block C-1 was made onto a plane dipping 50° southwest with strike normal to the cross projection, as shown in Figure 11. This slanted projection shows that the relatively high activity in the eastern belt is centered along a narrow band

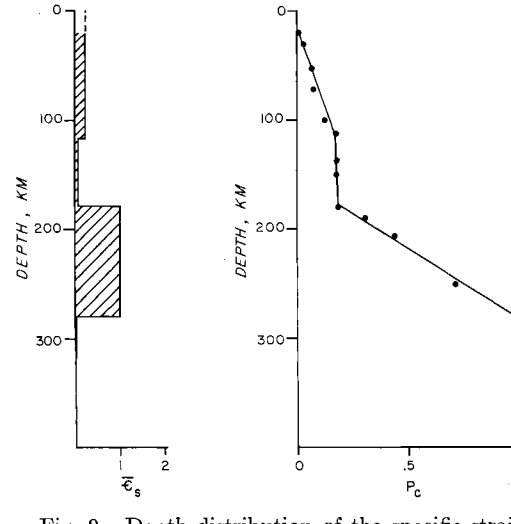

Fig. 9. Depth distribution of the specific strain release, eastern belt, block C-2, in units of $\Sigma N_4^{1/2}$ per unit volume per year. Unit volume is the same as in Figure 6. *Left,* average specific strain release. *Right,* cumulative plot of the specific strain release.

about 80 km wide (measured on the slanted plane) consisting of high-activity centers close together and nearly parallel to the auxiliary axis, which is the surface trace of the projection plane. This axis is located 320 km northeast of the western limit of C-1. It is surprising that no fault-plane solutions have ever been made within this belt. However, Hodgson (in *Byerly* [1955]) reported a fault-plane solution for a 1942 earthquake occurring in the zone between the major belts. This solution is shown in Figure 11, with the reported dip. The azimuth from the fault-plane solution and the general trend of C-1's activity agree well.

The projection plane of C-2's eastern belt (Figure 12) dips 50° southwest. Its auxiliary axis is located about 420 km northeast of the western side of C-2 (Figure 1), and is normal to the cross-projection plane (Figure 5). The data used in the construction of this slanted projection exclude the activity within 100 km of the western belt. In Figure 12 the activity resolves into a long high-activity center near the bottom of the figure, which is aligned with

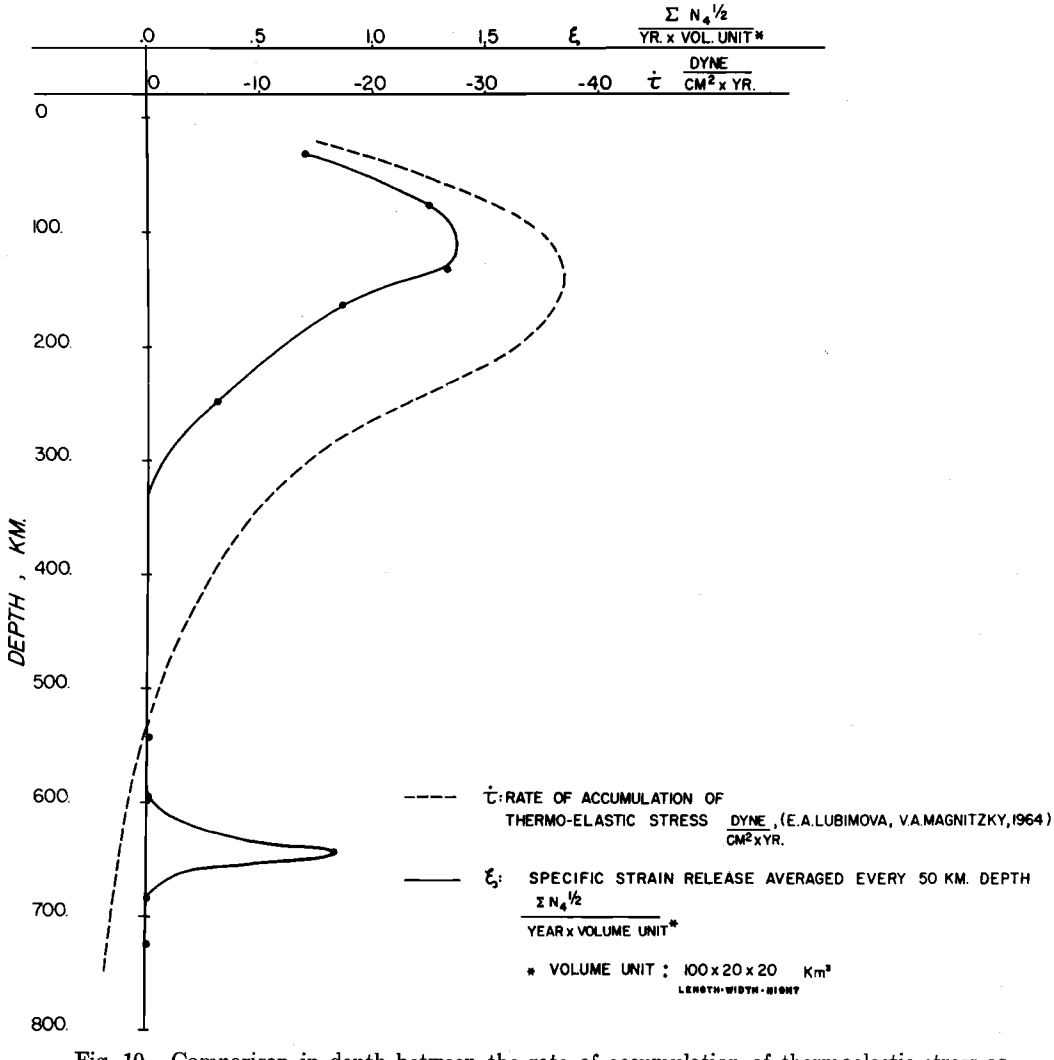

Fig. 10. Comparison in depth between the rate of accumulation of thermoelastic stress as computed by *Lubimova and Magnitzky* [1964] and the specific strain release averaged every 50 km of depth.

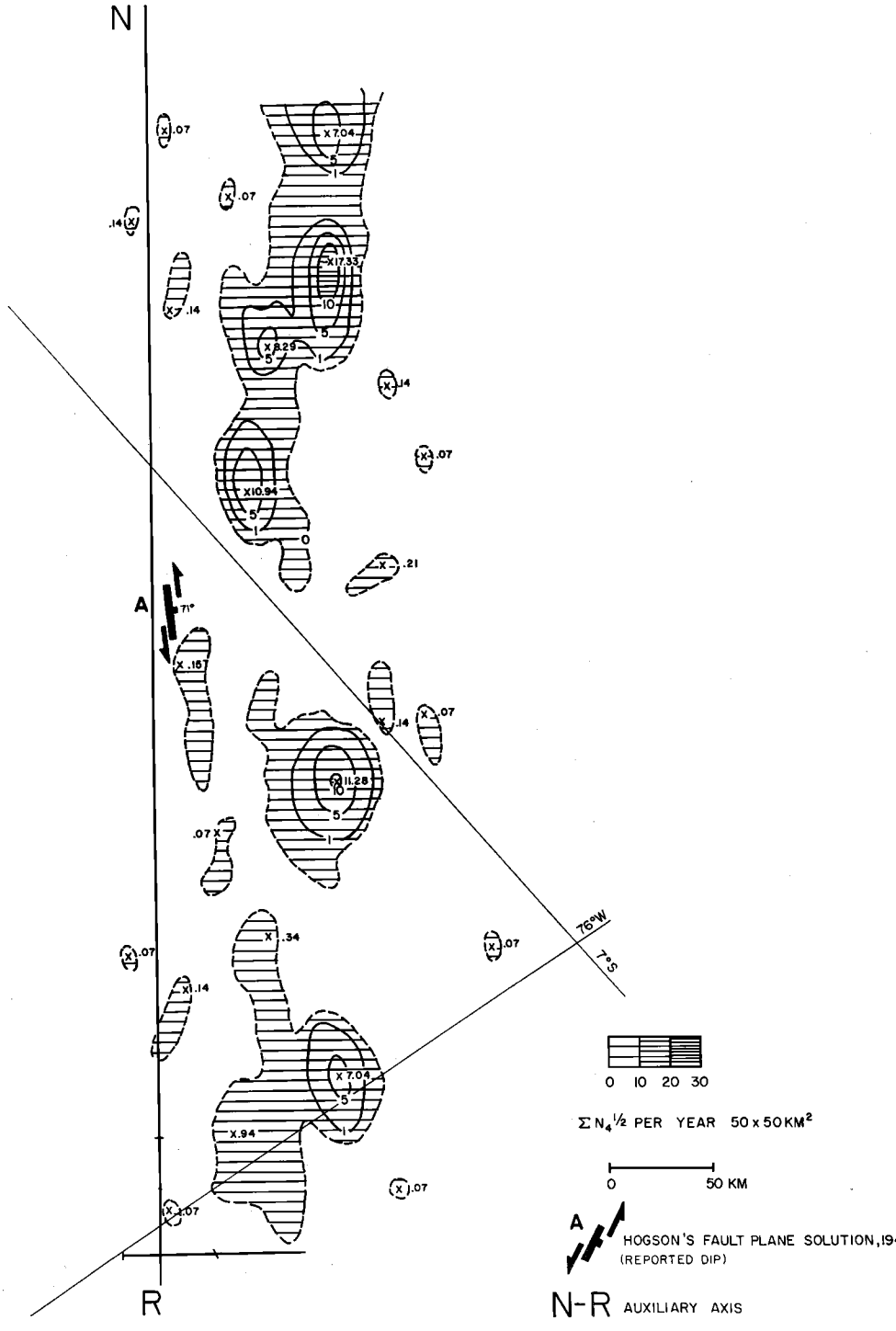

Fig. 11. Projection of the strain release on a plane dipping 50° southwest, eastern belt, block C–1. The auxiliary axis *N-R* is common for both belts within the block.

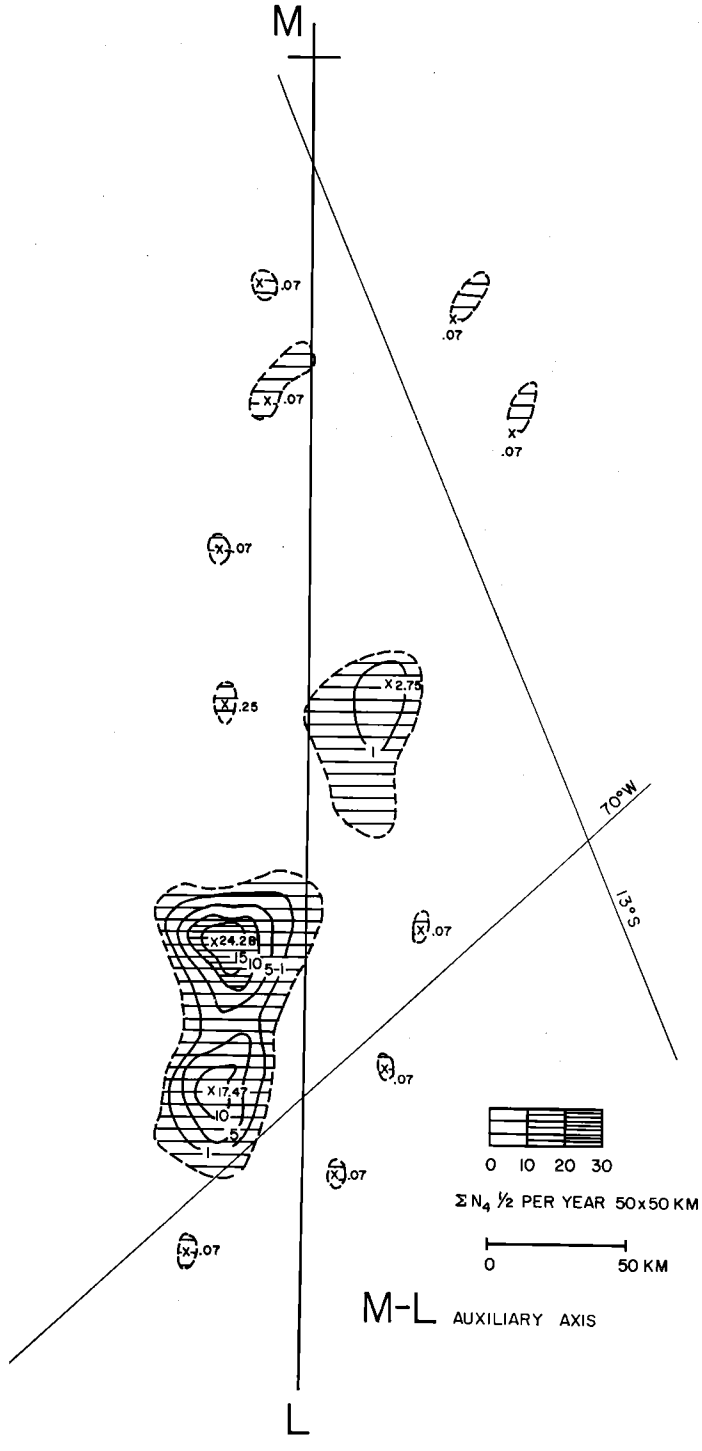

Fig. 12. Projection of the strain release on a plane dipping 50° southwest, eastern belt, block, C–2. The auxiliary axis M-L is common for both belts within the block.

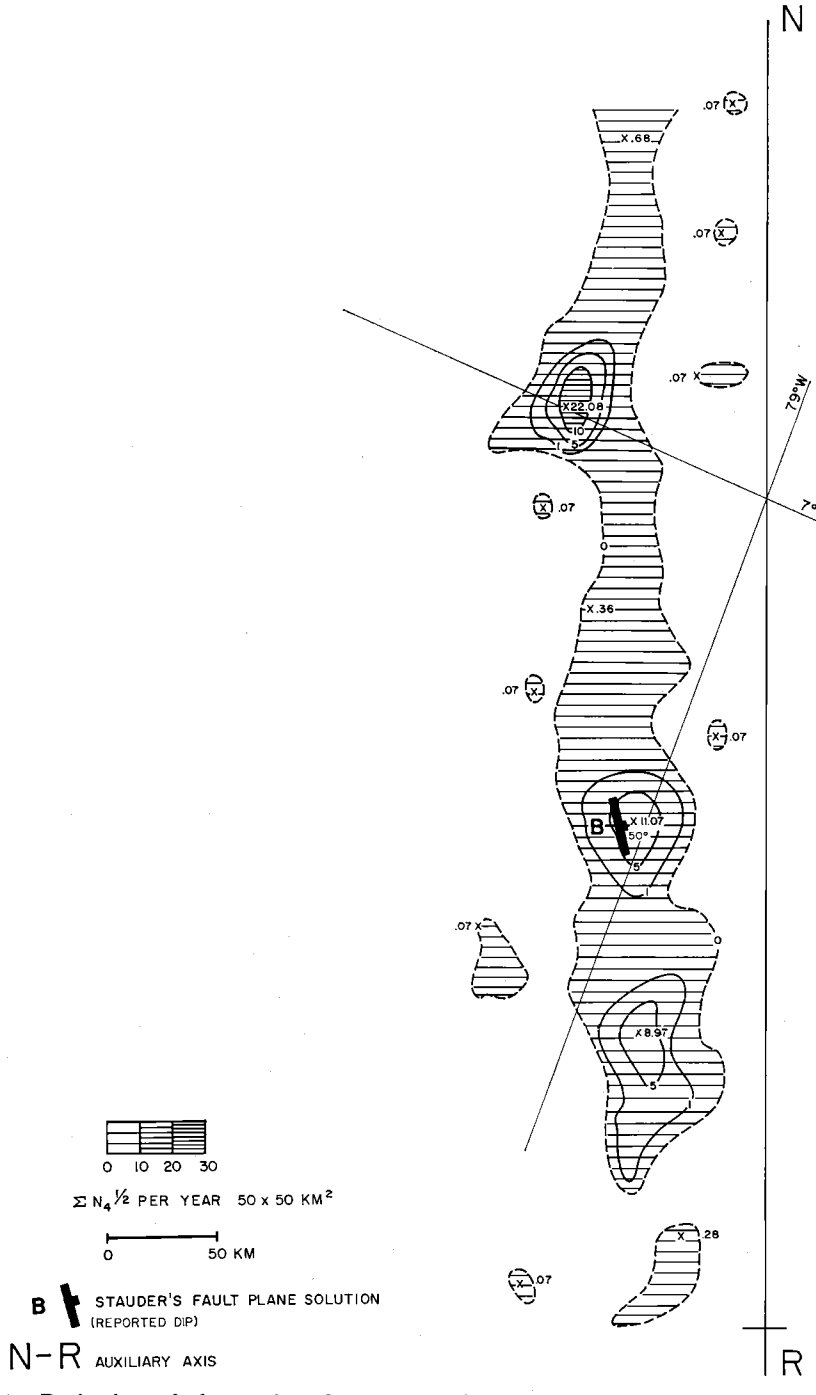

Fig. 13. Projection of the strain release on a plane dipping 30° southwest, western belt, block, C–1. The line *N-R* is an auxiliary axis common for both belts within the same block.

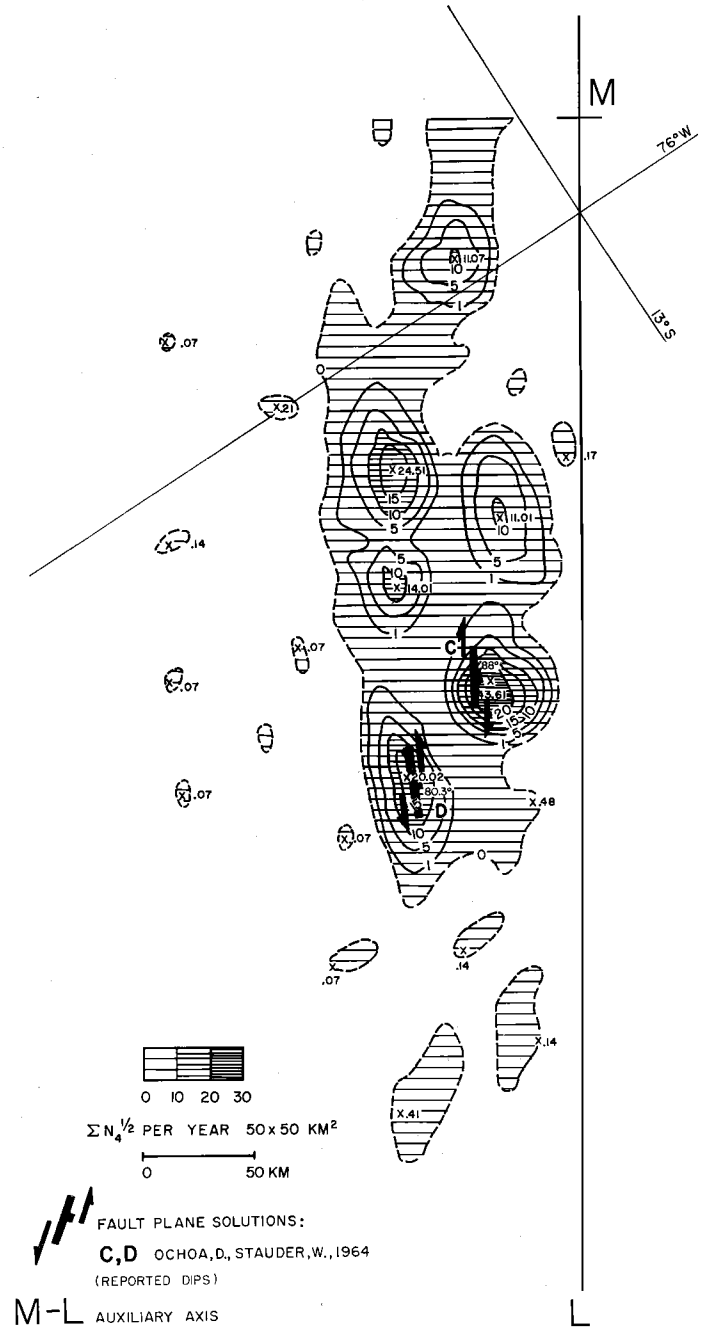

Fig. 14. Projection of the strain release on a plane dipping 15° southwest, western belt, block C–2. The line *M-L* is an auxiliary axis common for both belts within the block.

a few low-activity centers toward the top. There are no fault-plane solutions for this belt.

Figure 13 contains the projection of C-1's western belt onto a plane dipping 30° southwest. The auxiliary axis is the same as in Figure 11. Seismic activity is concentrated along a band 70–80 km wide (measured on the slanted plane), nearly paralleling the auxiliary axis. The one fault-plane solution made within this belt (William Stauder, S.J., 1965, personal communication) agrees within 10° in azimuth and dip with the general trend of the activity bands.

The western belt, block C-2, was projected onto a plane dipping 15° northeast (Figure 14), with the same auxiliary axis as in Figure 12. Seismic activity is concentrated in a narrow band 50–100 km wide (measured on the slanted plane). It displays two distinct alignments of high seismic activity centers, almost paralleling the auxiliary axis. A fault-plane solution is associated with each of the alignments, and they are shown, with the reported dips, in the figure. The azimuth and dip from the fault-plane solution are within the range estimated for this belt.

From these four figures we may conclude that the western belt in C-1 seems to be associated with a single band of activity which lies mostly under the continental shelf. Its counterpart in C-2 shows twin activity bands which parallel each other and lie mainly under the emerged continent, close to the coastline. The orientation of these high-activity bands shows good correlation with fault-plane solutions. The eastern band in C-1 seems to be related to a 'complex single band source' or very close 'twin band sources' of activity. But the counterpart in block C-2 does not clearly show the outline of the underlying 'energy source or sources.'

CONCLUSIONS

1. The strain energy release distribution with depth of the earthquakes within each seismic belt can be reasonably well described by layers of approximately constant strain release.

2. The classical picture of the distribution of earthquakes with depth is not verified in Peru, where we find a multiplicity of belts with varying dips within the first 300 km, earthquakes shallower than 70 km under the entire Andean block, a hiatus of activity between about 300 and 500 km, and a tendency toward horizontal distribution of the high seismic activity associated with the deepest shocks.

3. The existence of a multiplicity of high-activity bands within a belt explains the apparent inconsistency in fault-plane solutions for earthquakes located in the same area.

4. The theoretical rate of accumulation of thermoelastic strain release and the average rate of strain release are generally proportional in the upper 300 km. But thermoelasticity does not predict the increase of strain release associated with deep-focus earthquakes.

5. The phase change principally controlled by pressure seems to be the most likely mechanism to explain the deepest earthquakes, complemented by Orowan's creep instability mechanism.

Acknowledgments. I wish to express my appreciation to Professor Robert P. Meyer, of the University of Wisconsin, for his discussion and advice, and to Dr. Merle A. Tuve for his encouragement leading to my graduate studies. I am greatly indebted to the Carnegie Institution of Washington, the Geophysical Institute of Peru, and the Organization of American States for grants of fellowships which made possible the graduate work at the University of Wisconsin. I also thank the University of Wisconsin Computer Center for the use of its facilities, and the Wisconsin Alumni Research Foundation for its support.

This work was partly supported by National Science Foundation grant G.P. 2915.

REFERENCES

Benioff, H., Seismic evidence for the fault origin of the oceanic deeps, *Bull. Geol. Soc. Am., 60,* 1837–1856, 1949.

Benioff, H., Seismic evidence for crustal and tectonic activity, *Geol. Soc. Am. Spec. Paper 62,* 61–74, 1955.

Benioff, H., Source wave forms of three earthquakes, *Bull. Seismol. Soc. Am., 53,* 893–903, 1963.

Benioff, H., Earthquake source mechanism, *Science, 143*(3613), 1399–1406, 1964.

Byerly, P., Nature of faulting as deduced from seismograms, *Geol. Soc. Am. Spec. Paper 62,* 75–86, 1955.

Fisher, R. L., and W. R. Raitt, Topography and structure of the Peru-Chile Trench, *Deep Sea Res., 9,* 423–443, 1962.

Gutenberg, B. (editor), Evidence from deep focus earthquakes, *Internal Constitution of the Earth,* Dover Press, New York, 1951.

Gutenberg, B., and C. Richter, *Seismicity of the Earth and Associated Phenomena,* Princeton University Press, Princeton, N. J., 1954.

Gutenberg, B., and C. Richter, Great earthquakes, 1896–1903, *Trans. Am. Geophys. Union, 37,* 608–614, 1956*a*.

Gutenberg, B., and C. Richter, Earthquake magnitude, intensity, energy, and acceleration, 2, *Bull. Seismol. Soc. Am., 46*(2), 105–143, 1956*b*.

Hammond, C. S., *Hammond's Ambassador World Atlas,* Hammond Company, Maplewood, N. J., 1955.

Lubimova, E. A., and V. A. Magnitzky, Thermoelastic stresses and the energy of earthquakes, *J. Geophys. Res., 69*(16), 3443–3447, 1964.

Ochoa, D., and W. Stauder, The focal mechanism of two Peruvian earthquakes, *Pure Appl. Geophys., 58,* 114–122, 1964.

Ocola, L., Seismic activity of Peru: spatial distribution, M.S. thesis, University of Wisconsin, 1966.

Orowan, E., Mechanism of seismic faulting, *Geol. Soc. Am. Mem. 79,* 323–345, 1960.

Orowan, E., Continental drift and the origin of mountains, *Science, 146*(3647), 1003–1010, 1964.

Richter, C. F., An instrumental magnitude scale, *Bull. Seismol. Soc. Am., 25,* 1–25, 1935.

Ringwood, A. E., Mineralogical constitution of the deep mantle, *J. Geophys. Res., 67*(10), 4005–4010, 1962.

Rodríguez, A., J. Steinhart, and T. Asada, The San Agustín fault system of southern Peru, *Bull. Seismol. Soc. Am., 52*(4), 793–805, 1962.

Saint-Amand, P., Two proposed measures of seismicity, *Bull. Seismol. Soc. Am., 46*(1), 41–45, 1956.

Sclar, C. B., L. C. Carrison, and C. M. Schwartz, High-pressure reaction of clinoenstatite to forsterite plus stichovite, *J. Geophys. Res., 69*(2), 325–330, 1964.